Revista Facultad de Ingeniería

Title: **Obtaining materials from sargassum for use in an energy storage device**

Authors: Adriana Cervantes-Mendiola, Ulises León-Silva, María Elena Nicho, J. Jesús Escobedo-Alatorre, Jorge Arturo Sandoval-Espino, A. Olarte-Paredes and René Salgado-Delgado

DOI: **10.17533/udea.redin.20250775**

To appear in: *Revista Facultad de Ingeniería Universidad de Antioquia*

Received: June 12, 2024
Accepted: July 04, 2025
Available Online: July 04, 2025

Please cite this article as: A. Cervantes-Mendiola, U. León-Silva, M. E. Nicho, J. J.Escobedo-Alatorre, J. A. Sandoval-Espino, A. Olarte-Paredes and R. Salgado-Delgado. Obtaining materials from sargassum for use in an energy storage device, *Revista Facultad de Ingeniería Universidad de Antioquia*. [Online]. Available: https://www.doi.org/10.17533/udea.redin.20250775

Obtaining materials from sargassum for use in an energy storage device

Obtención de materiales del sargazo para su uso en un dispositivo de almacenamiento de energía

Adriana Cervantes-Mendiola[1] https://orcid.org/0000-0002-5440-0945, Ulises León-Silva[1*] https://orcid.org/0000-0003-0924-9980 *, María Elena Nicho[1] https://orcid.org/0000-0002-0835-0078, J. Jesús Escobedo-Alatorre[1] https://orcid.org/0000-0001-5281-0046, Jorge Arturo Sandoval-Espino[1] https://orcid.org/0000-0002-5743-9618, A. Olarte-Paredes[2] https://orcid.org/0000-0002-0959-6766 and René Salgado-Delgado[2] https://orcid.org/0000-0002-0313-6283

[1]Centro de Investigación en Ingeniería y Ciencias Aplicadas, Universidad Autónoma del Estado de Morelos. Av. Universidad 1001, Col. Chamilpa. C. P. 62209. Cuernavaca, Morelos, México.
[2]Tecnológico Nacional de México, Instituto Tecnológico de Zacatepec. Calzada Tecnológico # 27, Col. Centro. C. P. 62780. Zacatepec, Morelos, México.

Corresponding author: ulises.leon@uaem.mx

KEYWORDS
Extraction; Valorization; Energy storage; Electrochemical techniques
Extracción; Valorización; Almacenamiento de energía; Técnicas electroquímicas

ABSTRACT: Sargassum has become an “ecological disaster” on most beaches in the Caribbean Sea, causing serious health, safety, economic and environmental problems. The objective of this study was to valorize sargassum for the extraction of sodium alginate, cellulose and cellulose nanocrystals. Cellulose was also used in the manufacture of a separator for an energy storage device (ESD) based on expanded graphite and activated carbon. Sargassum was characterized physicochemically; the results of this characterization are very relevant for the generation of bioenergy and removal of toxic contaminants. The extracted materials were identified by FT-IR; the spectra were very similar to the IR spectra of commercial samples, which corroborated that the materials extracted were sodium alginate, cellulose and cellulose nanocrystals. The performance of the ESD/cellulose-based separator was determined using cyclic voltammetry (CV) and electrochemical impedance spectroscopy (EIS). Additionally, an RC circuit and an oscilloscope were used to perform a charge/discharge test. The voltammograms obtained for the ESD showed a rectangular shape with redox peaks characteristic of a pseudocapacitor and a battery, and the Nyquist plot showed a typical electrochemical performance of such ESD. Likewise, the developed devices have the capacity to store and release energy in seconds.

RESUMEN: El sargazo se ha convertido en un “desastre ecológico” en la mayoría de las playas del Mar Caribe, causando graves problemas de salud, seguridad, económicos y ambientales. El objetivo de este trabajo fue valorizar el sargazo para la extracción de alginato de sodio, celulosa y nanocristales de celulosa. Así mismo, la celulosa se utilizó en la fabricación de un separador para

un dispositivo de almacenamiento de energía (ESD) a base de grafito expandido y carbón activado. El sargazo se caracterizó fisicoquímicamente; los resultados de esta caracterización son muy relevantes para la generación de bioenergía y remoción de contaminantes tóxicos. Los materiales extraídos fueron identificados por FT-IR; los espectros fueron muy similares a los espectros IR de muestras comerciales, lo que corroboró que los materiales extraídos fueron alginato de sodio, celulosa y nanocristales de celulosa. El desempeño del ESD/separador a base de celulosa se determinó utilizando la voltamperometría cíclica (CV) y espectroscopía de impedancia electroquímica (EIS). Adicionalmente, se utilizó un circuito RC y un osciloscopio para realizar una prueba de carga/descarga. Los voltamogramas obtenidos para el ESD mostraron una forma rectangular con picos redox característicos de un pseudocapacitor y una batería, y el diagrama de Nyquist mostró un desempeño electroquímico típico de dicho ESD. Así mismo, los dispositivos desarrollados tienen la capacidad de almacenar y liberar energía en segundos.

1. Introduction

In 2011, a massive amount of sargassum (*Sargassum fluitans* and *Sargassum natans*, the most abundant species) was observed for the first time in the Atlantic Ocean. Since then, the massive arrival has continued to spread to form the "Great Atlantic Sargassum Belt" (GASB), which exceeded 20 million tons of biomass transported in June 2018 [1]. In the Mexican Caribbean, the massive arrival of sargassum began at the end of 2014, causing serious consequences not only at an ecological level, but also in the economic and social sphere. The costs related to sargassum cleaning range from 0.3 to 1.1 million dollars per kilometer and the amount of biomass collected annually ranges between 10,105 and 40,935 m^3 per kilometer [2]. Currently, the efforts made to prevent the arrival of sargassum to beaches have not been sufficient, and poorly executed cleaning practices cause the accumulation of decomposing biomass that depletes oxygen, reduces light, and deteriorates water quality [3]. For this reason, it is necessary and imperative to develop strategies associated with the treatment, recycling, and use of sargassum to counteract the negative impact that this macroalga has generated and thereby transform this serious problem into a technological and economic opportunity [4]. The valorization of sargassum represents one of the most viable options to economically benefit this resource because it offers a renewable source in the production of materials that can be used in various industries and technologies due to their properties, chemical compounds, and inorganic elements [5]. Among these materials are sodium alginate, cellulose, and cellulose nanocrystals.

Sodium alginate can form gels and is biocompatible; thus, it is considered an attractive product with a wide field of applications, such as a gelling agent, thickener, and stabilizer in the cosmetic, textile, pharmaceutical, and food industries [6,7] . In 2020, the size of the global alginate market was valued at 728.4 million dollars [8]. On the other hand, cellulose is the most abundant biopolymer available in nature since it is one of the main components of the cell walls of most plants [9]. In recent years, interest in cellulose, mostly at the nanometric scale, has increased with

the development of nanotechnology in the industrial sector because it is a green renewable material with good mechanical, physical, chemical, and thermal properties and of low-cost . These properties have allowed cellulose to be widely used for the manufacture of filters, separators, capacitors, supercapacitors, electrodes, [10–12], sensors [13], food packaging, polymer additives [14], among others.

Supercapacitors, pseudocapacitors and batteries are energy storage devices (ESDs) that will play a very important role in the following generations due to the development of technology, especially in "electronic mobility". These devices are made up of two current collectors with porous electrodes separated by a semi-permeable membrane (separator). The porous electrodes and separator are impregnated with an electrolyte [15]. It is worth mentioning that the role of the separator is very important for the operation of ESDs because it allows the passage of ions and prevents the passage of electrons.

The use of cellulose and cellulose nanocrystals for the manufacture of ESDs has been the focus of scientific study and previously reported. In a study, the development of supercapacitor electrodes based on activated carbon, graphite and cellulose nanocrystals (CNC) and CNC/glycerol/NaCl as electrolyte/separator was reported. The devices with these components presented a capacitance of 25.6 F g^{-1} at an operating voltage up to 1.2 V [16]. In another study, cellulose acetate (CA) and polystyrene (PS) composite for the manufacture of a separator was reported. The flexible supercapacitors manufactured with CA/PS composite presented specific capacitance values of 2.8 Fg^{-1} and 33 Fg^{-1} for electrodes with pristine carbon and PEDOT functionalized carbon fibers, respectively [17]. Moreover, [18] reports the development of a cellulose/PEDOT:PSS composite matrix adding multi-walled carbon nanotubes (MWCNTs) to it, thus improving the flexibility and electrical conductivity of the composite matrix. The supercapacitor assembled with MWCNT/composite matrix as electrodes achieved a high specific capacitance of 485 F g^{-1}. In [19], researchers developed an anthraquinone sulfonate-doped PPy/cellulose fiber electrode material for the fabrication of supercapacitors. This device showed a high capacitance of 829.8 F g^{-1}. Likewise, [20] reports manufacturing cellulose nanofibers/reduced graphene oxide/polypyrrole (CNF-RGO-PPy) paper electrode materials with a sandwich structure. The porous structure of the CNF/RGO layer and the pseudocapacitance characteristics of PPy enabled excellent specific capacitance (195.8 F g^{-1}) in the supercapacitor. Also, in [21], a dual-physical crosslinking carboxymethyl cellulose hydrogel with high toughness, healability, and electric conductivity for the manufacturing of supercapacitors has been developed. The devices showed a high specific capacitance of 309 F g^{-1}.

In this study, sodium alginate, cellulose and cellulose nanocrystals were obtained from sargassum through a thermochemical process based on literature reports, in which reaction times, temperatures, and concentrations of the reactants were modified. Likewise, cellulose was used to manufacture a separator for an ESD based on expanded graphite and activated carbon. The performance of the ESD manufactured with the cellulose-based separator was determined using electrochemical techniques. The results obtained show that the valorization of sargassum for the

extraction of sodium alginate, cellulose and cellulose nanocrystals is feasible. Likewise, the electrochemical performance of the ESD/cellulose-based separator was very promising, obtaining specific capacitance values and electrochemical behavior like those reported for devices manufactured with commercial separators. This opens an opportunity to use sargassum for the development of more sustainable technology that allows for optimal use of resources, contributes to a possible reduction in poverty, generates jobs, promotes the circular economy and, improves energy efficiency.

2. Experimental section

2.1. Sargassum conditioning

The sargassum (**Figure 1**) was collected on the beaches of the Mexican Caribbean. The macroalgae were washed and cleaned manually with tap water to remove waste (sand, plastics, etc.). Subsequently, it was dried at room temperature for 24 h to eliminate residual moisture. Finally, the sargassum was crushed manually using a mortar and airtight stored in the refrigerator for 24 h.

Figure 1 Sargassum collected from the beaches of the Mexican Caribbean.

2.2. Physicochemical characterization

The physicochemical characterization of sargassum consisted of an elemental analysis through atomic absorption spectroscopy of 17 chemical elements, the determination of the sodium chloride (NaCl) content, higher heating value (HHV), sulfur (S) content, humidity, ash and volatile material, and pH value. Atomic absorption spectrophotometry (AAS, Varian SpectrAA 220FS) with electrode discharge lamps and air/acetylene flame was used for the determination of chemical elements. Calibration standards series were prepared for each element by dilution.

The HHV was determined using a bomb calorimeter (IKA, C200) according to ASTM D5865; the samples were previously dried at 105 °C for 24 h. Approximately 0.8 g of each sargassum sample was used for analysis, in triplicate. The sulfur (S) content was determined using a carbon and sulfur

analyzer (Infrared, QT-CS-3000G QUALITEST). Muffle furnaces and incineration crucibles were used to determine ash content according to ASTM E1755; porcelain crucibles were heated at 575 °C for 3 h. They were allowed to cool until they reached room temperature, and then weighed (empty crucible mass). Subsequently, 1 g of sargassum was added to the crucibles and heated at 250 °C for 30 min. Then, the samples were heated at 575 °C for 1 h. Finally, the crucibles were allowed to cool until they reached room temperature. A vertical tube furnace/platinum crucible was used to determine volatile matter according to ASTM D3175; the sargassum sample was pulverized to a 250 µm sieve and 1 g at 950 °C was used for the test. In addition, FT-IR spectroscopy analysis was carried out for the identification of the extracted materials using the Bruker Equinox 55 model (attenuated total reflection mode); 64 interferograms were recorded with a resolution of 2 cm^{-1}.

2.3. Sodium alginate extraction

Sodium alginate extraction was conducted following the protocols of [22] and [23] with modifications in reaction times, concentrations, and temperature. The extraction was carried out through two different processes with the aim of obtaining a higher yield:

Process 1. 10 g of sargassum were treated with 400 mL of 2% furaldehyde at room temperature for 24 h to eliminate soluble resinous components. Subsequently, the solid was treated with 400 mL of 0.1M hydrochloric acid (HCl) while stirring at room temperature for 16 h. Then, it was adjusted to a neutral pH using distilled water and filtered to separate the solid. Subsequently, the solid was treated with 400 mL of 2% sodium carbonate (Na_2CO_3) at 60 °C for 3 h to extract the sodium alginate, which was separated from the solid material by filtration. Finally, the sodium alginate in solution was precipitated in ethanol; the sodium alginate fibers are shown in **Figure 2**.

Figure 2 Sodium alginate fibers.

Process 2. 10 g of sargassum were treated with 500 mL of sodium hypochlorite (NaClO) at room temperature for 10 min to bleach and extract the lignin present. The solid was then filtered, washed with tap water to remove residual chlorine, and dried at room temperature for 10 h. Subsequently, the bleached solid was treated with 350 mL of 0.1 M HCl at room temperature for 16 h to form alginic acid. Then, the solution was filtered and the solid was washed with distilled water until reaching a neutral pH. Subsequently, the solid was treated with 350 mL of 2% (Na_2CO_3) for 3 h at 60 °C to obtain sodium alginate; the solid was filtered to obtain sodium alginate in solution. Finally, the sodium alginate solution was precipitated over ethanol, filtered, and oven-dried at 45 °C for 2 h; the sodium alginate is shown in **Figure 3**.

Figure 3. Bleached sodium alginate.

2.4. Cellulose and cellulose nanocrystals extraction

Cellulose and cellulose nanocrystals extractions were conducted following the protocols of [24] and [25] with minimal modifications in concentrations and reaction times. Cellulose extraction was carried out as follows: 10 g of sargassum was bleached with 500 mL of NaClO at room temperature for 3 h. Subsequently, the solid was filtered and washed with distilled water to remove residual NaClO. Then, the solid was treated with 750 mL of 0.5 M sodium hydroxide (NaOH) at 80 °C for 3 h to eliminate lignin; the treatment was carried out twice. The solid was filtered and washed with distilled water until reaching neutral pH. Then, the solid was treated with 250 mL of 0.05M HCl at room temperature for 24 h to eliminate hemicellulose. Finally, the solid was filtered and washed with distilled water until reaching a neutral pH and dried at 40 °C for 2 h; the cellulose is shown in **Figure 4**.

Figure 4 Cellulose from sargassum.

Cellulose nanocrystals extraction was carried out as follows: 3.5 g of cellulose was treated with 60 mL of 64% sulfuric acid (H_2SO_4) at 45°C for 45 min. Subsequently, the product was poured onto 1.5 L of cold distilled water and kept at rest for 2 h to later separate the phases by decantation; this was done twice. Then, the solution containing the cellulose nanocrystals was dialyzed to neutralize it. Subsequently, the cellulose nanocrystals were treated by ultrasound (avoiding overheating) until obtaining a colloidal solution; this solution was filtered using vacuum and a glass microfiber membrane (280 mL of cellulose nanocrystals in solution were obtained). Finally, 50 mL of cellulose nanocrystals in solution were dried at 40 °C for 24 h; cellulose nanocrystals film with a weight of 0.3046 g was obtained (1.9073 g of cellulose nanocrystals dissolved in 280 mL of colloidal solution). The cellulose nanocrystals film is shown in **Figure 5**.

Figure 5 Cellulose nanocrystals film from sargassum.

2.5. Morphology of nanocrystalline cellulose and cellulose

Transmission electron microscope (TEM) observation of the resultant cellulose nanofibers was performed on a FEI-TITAN TEM with an energy of 80 kV. The diluted cellulose nanofibers were dropped on a holey carbon-coated TEM support grid, and then negatively stained by 1 % tungstophosphoric acid (TPA) solution. The surface morphology of the cellulose separator was investigated by scanning electron microscopy (SEM, JEOL JSM-6010LA). The cellulose separator was placed on carbon tape and performed with coating. The images obtained were analyzed using ImageJ software.

2.6. Manufacturing of the cellulose-based separator

The cellulose-based separator was manufactured as follows: the extracted cellulose was cut into small pieces and placed in a container with distilled water for 24 h. Then, cellulose in distilled water was liquefied until obtaining a, homogeneous mixture. Subsequently, the mixture was poured into a mesh rack and distributed evenly with a sponge; this allowed excess water to be removed. Then, an absorbent cloth was placed over the mixture and pressed to remove more water. Subsequently, the cellulose was carefully removed from the mesh rack and placed on a type C press for 2 h. Finally, the cellulose was removed from the press and dried at room temperature for 24 h. Using a MITUTOYO micrometer, three measurements were made of the cellulose-based separator, with the average thickness being calculated at 415 μm. The cellulose-based separator is shown in **Figure 6**.

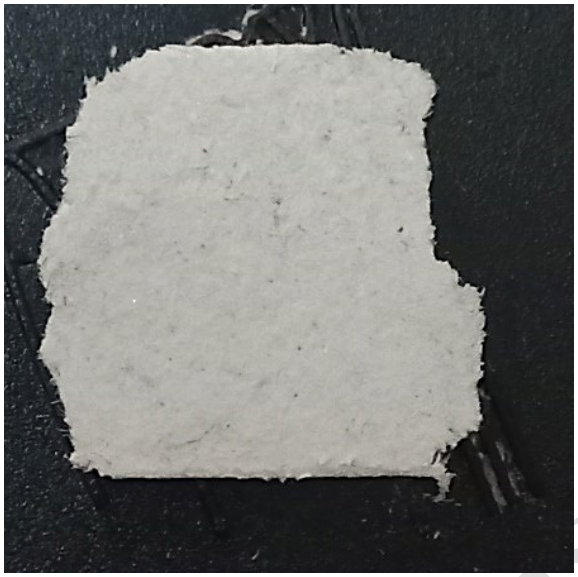

Figure 6 Cellulose membrane.

2.7. Manufacturing of energy storage devices

The manufacturing of the devices was carried out as follows: the cellulose-based separator was cut into 1×1 cm sheets. Then, a mixture (0.023 g) of commercial activated carbon (Herbonaturista, 95 wt%) and commercial expanded graphite (Timrex BNB90, specific surface area = 21.2 m^2/g, 5 wt%) was added into one of the copper collectors (thickness = 20 μm). Subsequently, the cellulose-based separator was placed and 5 drops (standard measurement) of 3 M KOH (electrolyte) were added. Finally, the mixture (0.023 g) of activated carbon (95% by weight) + expanded graphite (5% by weight) was added to the cellulose-based separator and the other copper collector was placed. **Figure 7** shows a scheme of the manufactured energy storage device; this device had an effective area = 1 cm^2.

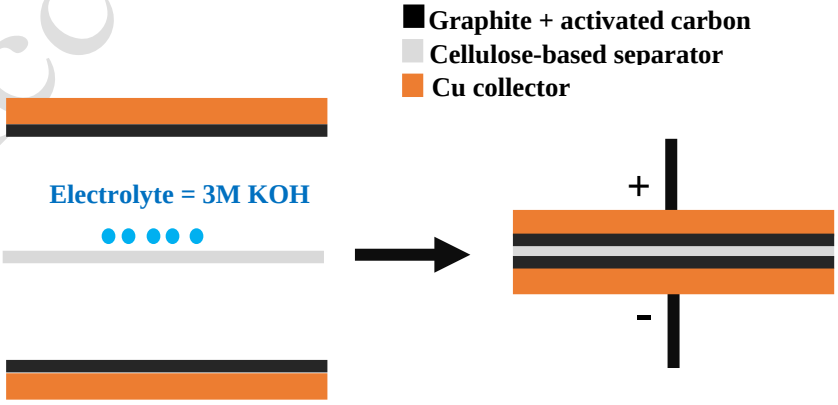

Figure 7 Scheme of manufactured energy storage devices.

2.8. Electrochemical and electrical characterization of energy storage device

For the electrochemical characterization of the ESD, a two-electrode cell (Figure 7) connected to a GILL AC potentiostat/galvanostat (ACM Instruments) was used. The ESD was characterized by electrochemical impedance spectroscopy (EIS) using an AC potential amplitude of 10 mV, a frequency range of 10 mHz to 30 kHz with 100 readings per decade and the device was under zero polarization at room temperature during the EIS tests. Likewise, ESD was characterized by cyclic voltammetry (CV) at different rates: 10, 20, 50 and 100 mV s^{-1} and a potential window of -1 to 1 V. The specific capacitance through CV (C_{CV}) was determined using **Equation 1** [26]:

$$C_{CV} = \frac{\int_{V_1}^{V_2} I(V)dV}{v \times \Delta V \times m} \quad (1)$$

Where C_{CV} is the specific capacitance at Fg^{-1}, v is the scanning speed in V/s, m is the mass of the active material in g, ΔV is the potential window in V and IdV represents the area under the CV curve.

A charge/discharge test was also carried out to confirm that the device-stored energy. The circuit in **Figure 8** was built with physical components; an RC circuit was connected to a direct current (DC) power supply.

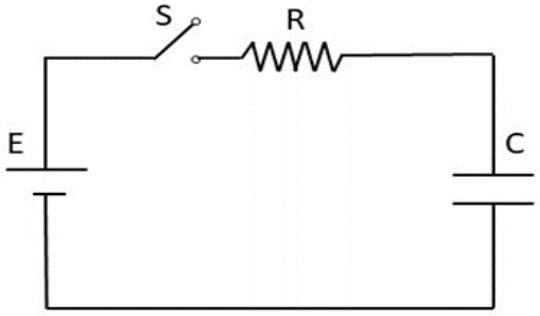

Figure 8 RC electrical circuit. E= DC supply voltage, R= resistance, and C (capacitor) in this study is the ESD.

When switch S is activated, the transient charging phase of the capacitor begins, which is determined by Equation 2.

$$V_C = E(1 - e^{-\frac{t}{RC}}) \quad (2)$$

From (2), the capacitance of the ESD (C_{ESD}) can be calculated at any time *t* during the transient charging phase (Equation 3).

$$C_{ESD} = t/[R \times \ln\left(\frac{E}{E-V_c}\right)] \quad (3)$$

The charge and discharge test was performed by measuring the signal with a TEKTRONIX oscilloscope at a sampling rate of 1 MS s^{-1}. Then, according to (2), when $RC = t$, the voltage value V_C will be 63.2% of the voltage *E*, as expressed in Equation 4.

$$V_C = E\left(1 - exp^{-\frac{t}{t}}\right) = E(1 - exp^{-1}) = E(0.632) \quad (4)$$

The calculation of C_{ESD} was carried out at 63.2% of the maximum charging voltage. Based on the waveform acquired by the oscilloscope and the sampling frequency, the time in which the V_C voltage reached 63.2% in *E* was determined. These values were then substituted into (3) to calculate C_{ESD}. The applied voltage was 2 V, 10 kohms resistance and frequency of 1 MHz were used.

3. Results and discussion

The elements found in sargassum are presented in **Table 1**. These elements have been reported in the literature [27] for Sargassum fluitans and Sargassum natans. Mg, Ni, Cr and Zn were the elements found in the highest concentration. Most of these elements are essential nutrients; others are highly toxic to humans, animals, and the environment, such as arsenic, cadmium, mercury, and lead [28].

Table 1 Content of the elements in the sargassum.

	Sargassum	
Element	**ppm**	**%**
Copper	9.7	0.0010
Magnesium	45	0.0045
Lead	6.0	0.0006
Cadmium	4.3	0.0004
Nickel	39	0.0039
Cobalt	4.7	0.0005
Chrome	42	0.0042
Zinc	22	0.0022
Vanadium	<5	<0.0005
Barium	<200	<0.02
Beryllium	<2	<0.0002
Antimony	<3	<0.0003

Arsenic	<47	<0.0047
Selenium	<54	<0.0054
Tin	<8	<0.0008
Mercury	<0.003	<3E-7

Likewise, the sargassum contained chlorine and sodium chloride (NaCl) as expected when coming from the sea; see **Table 2**.

Table 2 Total chlorine and sodium chloride content.

	Sargassum
Total chlorine	14.39%
NaCl	159 mg/g sample

Other physicochemical results of sargassum that are of great interest to the bioenergy generation industry are presented in **Table 3**. In thermochemical conversion routes, an important basic property is the higher heating value (HHV). The sargassum analyzed has a HHV value of 1.09×10^7 J/kg. In comparison, a variety of materials widely used in the generation of bioenergy have been reported in the literature; for example, tepa, rauli and hazelnut woods have HHV values between 1.84×10^7 and 2.12×10^7 J/kg, olivillo wood between 8.37×10^5 and 1.67×10^6 J/kg [29], hops 1.95×10^7 J/kg [30], and some species of brown macroalgae such as *Sargassum vesigoso*, *Chorda filum* and *Laminaria digitata*, 1.49×10^7, 1.55×10^7, and 1.75×10^7 J/kg, respectively [31]. These are comparable to the HHV value for the sargassum, which means it could also be used for the generation of bioenergy. On the other hand, for the energy recovery of sargassum, the moisture content was very high since it is greater than 7% (reference value), which indicates that it could not be used in international markets [32]. Likewise, the percentage of volatile material for sargassum was very low (7.71 %) compared to high quality materials for energy recovery purposes; for example, charcoal from *Quercus sp* has a percentage of volatile material of approximately 15%, which allows rapid ignition, presence of flame and high spark production. The ash content in sargassum was very high, taking 6% or < 6% as acceptable values [33]. This attribute of sargassum is undesirable because its residue (ash) would accumulate in the equipment.

Regarding the sulfur content in the decomposition of sargassum (**Table 3**), this element is released into the water producing hydrogen sulfide, which causes pollution in both the water and the atmosphere [34]. On the other hand, the pH of 7.77 in sargassum is highly desired for the removal of toxic contaminants from aquatic environments because lower pH values cause repulsion between protonated carboxylic acids and heavy metal cations leading to a low adsorption capacity and higher pH values of deprotonate hydroxyl, amines, and carboxyl functional groups resulting in the precipitation of hydroxide anionic complexes that prevent efficient adsorption [35].

Table 3 Other physicochemical results.

	Sargassum
Higher heating value (J/kg) db**	$1.09\times10^{7}\pm1\times10^{5}$
Moisture (%wt.)	16.65 ± 0.36
Ash (%wt.)	32.80 ± 0.61
Volatile material (%wt.) mafb***	7.71 ± 0.67
Sulfur (%wt.)	1.17 ± 0.02
pH	7.78

db**: dry base. mafb***: moisture and ash free base.

The yields obtained in the two processes for the extraction of sodium alginate were 20 and 39% for *Processes 1* and *2*,, respectively. The bleaching of sargassum with sodium hypochlorite allowed a higher yield. This could be because bleaching can lead to a decrease in molecular weight and rheological properties in sargassum due to glycosidic bond degradation, which may be related to the yield obtained in the process. In the literature, the sodium alginate obtention from *Sargassum echinocarphum* with a yield of 32.42 % has been reported [22]. Likewise, the yields obtained in the extraction of cellulose and cellulose nanocrystals were 13 and 37%, respectively. These yields are very promising in comparison with some reports in literature: in [36], the extracted cellulose yield varied between 11.70% for *Colpomenia sinuosa* and 1.38% for *Jania rubens*. Likewise, [3] reported the cellulose nanocrystals obtention from a mix of *Sargassum spp.* yielding 14.9 %.

The extracted materials were characterized by FT-IR to identify their functional groups; IR spectra were compared with IR spectra of commercial samples of sodium alginate, cellulose and cellulose nanocrystals. In **Figures 9** and **10**, the spectra of commercial sodium alginate and the materials obtained in processes 1 and 2, respectively are shown. According to one study reported in the literature, the characteristic absorption peaks of sodium alginate are found at 3250, 2940, 1600, 1410 and 1020 cm^{-1} [37]. However, in another study the characteristic absorption peaks of sodium alginate are found at 3440, 1610 and 1089 cm^{-1} [38]. In both samples, the absorption peak around 3250 or 3440 cm^{-1} assigned to the O-H stretching vibration was observed. However, the lowest intensity absorption peak at 2924 cm^{-1} attributed to the C-H stretching vibration was observed in the *Process 1* sample, but not in the *Process 2* sample. The absorption peak at 1593 cm^{-1} corresponds to the asymmetric vibration of the carboxylate group, which could be observed in the

sample from *Process 1*, while in the sample from *Process 2* it was observed in lower intensity and slightly shifted towards a higher wave number (1632 cm^{-1}). Asymmetric vibration at 1649 cm^{-1} for sodium alginate from Sigma has been reported by [39].The signal at 1406 cm^{-1} corresponding to the symmetric vibration of the carboxylate group was observed in the samples from the two processes. However, the absorption peak at 1025 cm^{-1} associated with the C-O-C stretching vibration from glycosides was observed only in the sample from *Process 1*. In the literature [40] it is reported that the presence of a peak at 1025 cm^{-1} in sodium alginate suggests that it is slightly richer in mannuronic residues than in guluronic residues. In the case of bleached sargassum, residues of sodium hypochlorite could have reacted with ethanol, preventing the efficient extraction of the glycosides compounds because the use of polar solvents such as ethanol, methanol, and water for the efficient extraction of phenolic compounds is reported in [40]. Likewise, the peaks observed in the extracted sodium alginate spectra but not in the commercial sodium alginate spectra could be explained by the presence of carboxylic acid esters [38, 41]. The FTIR spectra showed similarity between the extracted sodium alginate with the commercial sodium alginate indicating that the sodium alginate extracted from sargassum can be considered as candidates for industrial exploitation.

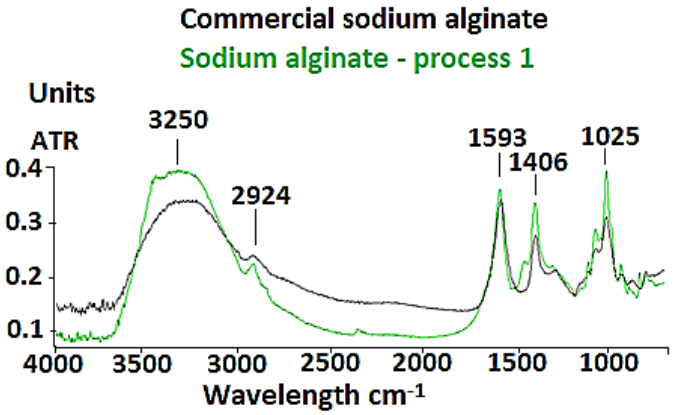

Figure 9 IR spectra of the material from *Process 1* (green color) and commercial sodium alginate (black color).

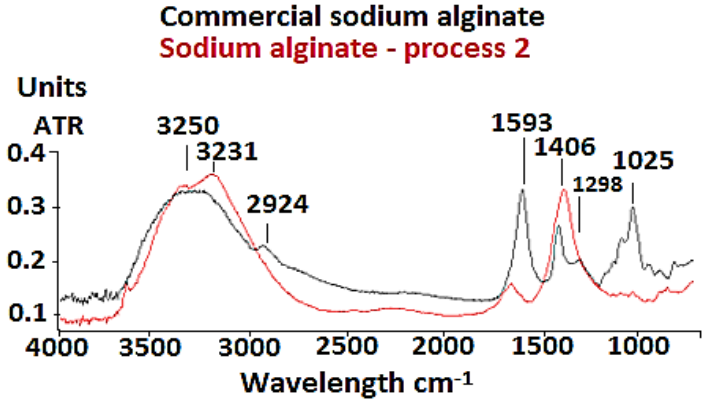

Figure 10 IR spectrum of the material from *Process 2* (red color) and commercial sodium alginate (black color).

Figures 11 and **12** show the FT-IR spectra of the "cellulose" and "cellulose nanocrystals" extracted from sargassum (blue spectrum) and the commercial cellulose and cellulose nanocrystals (red color). All spectra showed a broad strong band with two peaks at 3340 and 3282 cm^{-1} attributed to the stretching vibration of OH and N-H present in protein, respectively [42, 43]. In addition, other absorption peaks of lower intensity were observed at 2850 and 2918 cm^{-1} corresponding to the C-H stretching vibrations of the methyl and methylene functional groups, respectively [43]. Approximately in 1735 and 1638 cm^{-1}, two absorption peaks associated with the carboxylate groups due to the (C=O and N-H of the proteins, respectively,) were observed [43]. These peaks are more intense in the "cellulose" and "cellulose nanocrystals" extracted from sargassum and correspond to what was reported in reference [43], where the cellulose nanocrystals from *Sargassum spp* (yield of 14.9%) for the development of transparent films was characterized. Both spectra show the absorption peaks at 1052, and 1159 cm^{-1} attributed to the asymmetric C-O-C stretching and bending mode, respectively. The functional groups identified indicate that the materials obtained in the extractions are cellulose and cellulose nanocrystals.

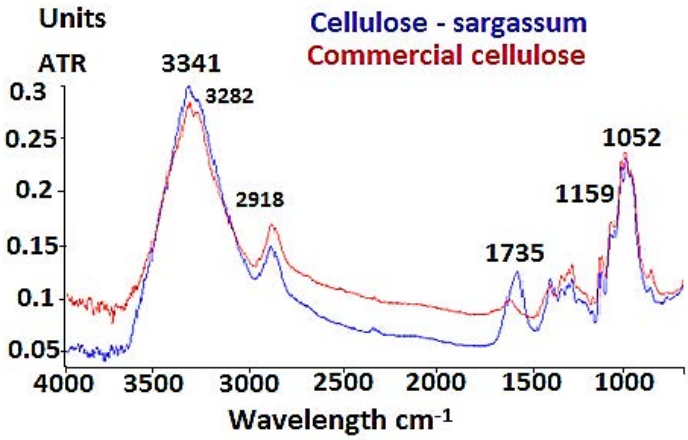

Figure 11 IR spectra of the cellulose extracted from sargassum (blue color) and the commercial sample (red color).

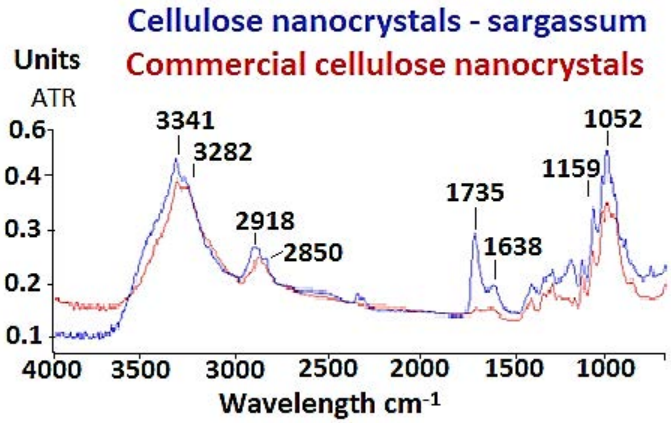

Figure 12 IR spectra of cellulose nanocrystals extracted from sargassum (blue color) and commercial cellulose nanocrystals (red color).

Figure 13 shows the SEM image of the cellulose separator having fiber diameters of 5 μm to 50 μm approx. The fibers are randomly distributed forming a nonwoven structure with high porosity and interconnected pores that could allow electrolyte flow. The separator had a rough fiber morphology. There are studies [44-46] that report the development of cellulose separator for supercapacitors and batteries with a morphology and fiber size like that reported in this work. However, the development of a separator of cellulose extracted from sargassum for ESD has not been reported. The diameters of these fibers were determined using ImageJ software.

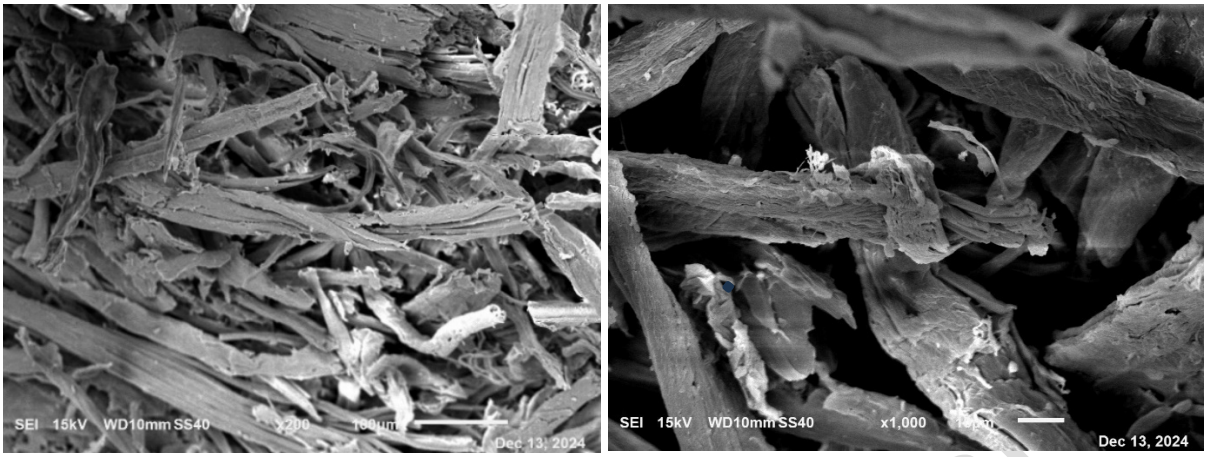

Figure 13. SEM images of cellulose separator at 200x (left) and 1000x (right).

Figure 14 shows the TEM image of cellulose nanocrystals. The cellulose nanocrystals were obtained in elongated filaments and showed a needle-crisscrossed structure with an average length and width between 120-130 nm and 5-8 nm, respectively. A similar structure has been reported using an ultrasonic homogenizer sonicator for size reduction of cellulose nanofibers from sargassum [47]. The length and width dimensions of these nanocrystals were determined using ImageJ software.

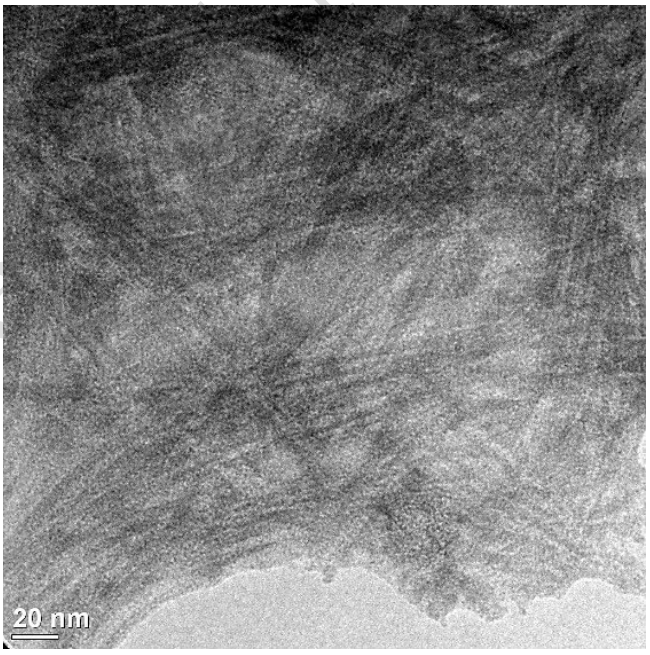

Figure 14. TEM image of cellulose nanocrystals.

Figure 15 shows the voltammograms of the ESD at different scan rates. It is important to mention that according to literature, the voltammogram of an ideal capacitor has a rectangular shape. Likewise, supercapacitors have a voltammogram with a quasi-rectangular shape [48]. In this study, all voltammograms showed a quasi-rectangular shape with peaks. These peaks are due to reversible redox reactions that occur at or near the surface of the electrode materials [49] and due to the rapid mobility of ions towards the electrode surface as the scan rate increased, altering the shape of the CV; ions can be considered to undergo intercalation/deintercalation [50]. The area under the oxidation and reduction peaks are not equal indicating similar kinetics of oxidation and reduction and facile electrochemistry with less polarization [48]. This behavior and the quasi-rectangular shape of the voltammogram are characteristic of ESDs called pseudocapacitors [51]. However, the shape of the voltammogram is also like that observed with batteries. The calculated specific capacitances (C_{CV}) were 17.3, 9.9, 5.1 and 3.6 Fg^{-1} at 10, 20, 50 and 100 mVs^{-1}, respectively. The values of C_{CV} indicate that the manufactured cellulose-based separator allows the correct operation of the ESD. Likewise, the performance of the pseudocapacitor is very promising compared to the performance of an ESD with a commercial polyvinylidene difluoride (PVDF)-based separator. C_{CV} values for ESDs/PVDF separators in the range of 16.1 to 107.6 Fg^{-1} using graphite, activated carbon and 3M KOH as electrolyte were reported in [52]. Likewise, values of specific capacitance of 25 - 30 Fg^{-1} were reported for commercial carbon-based supercapacitors [53].

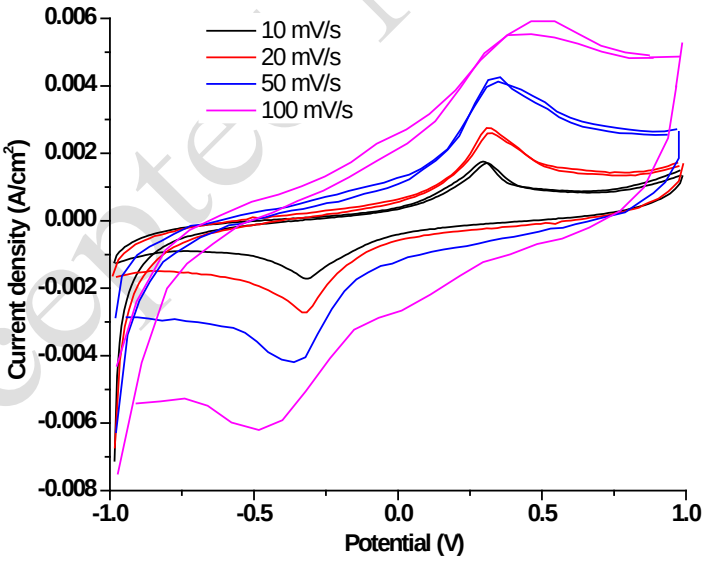

Figure 15 Voltammograms of the ESD at different scan rates in the 3M KOH electrolyte.

The Nyquist plot of the ESD based on graphite and activated carbon/ cellulose-based separator is shown in **Figure 16**. By taking the intercept with the Z_{real} axis of the semicircle at high frequency, the internal resistance known as equivalent series resistance (*ESR*) of the device can be estimated.

Low *ESR* is preferred for the device to perform better power transactions [54].
The first semicircle (high frequencies) corresponds to effects related to the electrolyte interface (EI), a passivation layer occurring on the electrode. The second semicircle (high-middle frequencies) displays the charge-transfer resistance (R_{ct}) and the influence of the double layer capacitance (C_{dl}) on the behavior of the energy storage device [55]. For materials with kinetically fast charge transfer, the diameter of the semicircle is very small [56]. At medium frequencies, a line with an angle of approximately 45° with respect to the Z_{real} axis was observed. This line is related to Warburg impedance (*W*) and is due to the diffusion of ions from the bulk [57]. It seems that is the behavior of a battery. However, the contribution at high and low frequencies indicates that the behavior is of a supercapacitor. A line with an angle greater than 45° with respect to the Z_{re} was observed at low frequencies due to the pseudocapacitive behavior of the device [58]; a vertical line (parallel to the Z_{im} axis) in the Nyquist plot is the behavior of an ideal capacitor.

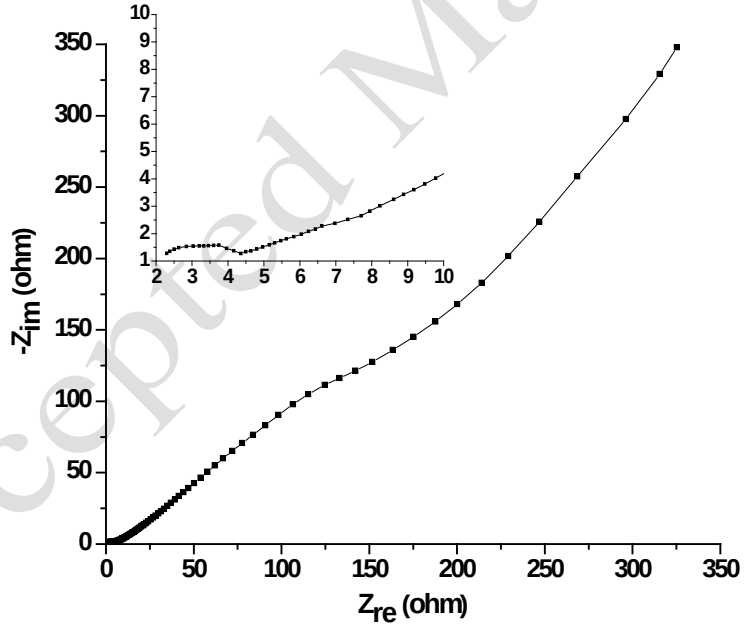

Figure 16 Nyquist plot of the ESD based on graphite and activated carbon with cellulose-based separator in the 3M KOH electrolyte. Insets show the plot at high frequencies and an equivalent circuit model.

The proposed equivalent circuit for the simulation of EIS data is presented in **Figure 16** (inset), which consists of the *ESR*, R_{EI}, CPE_{EI}, R_{ct}, CPE_{dl}, the pseudocapacitance (CPE_{ps}) and *W*, where *W* represents **Equation 5** [59]:

$$W_{(\omega)} = R_W[\coth(\omega\alpha)^s / (\omega\alpha)^s] \quad (5)$$

where ω is the frequency, R_W is the finite resistance at low-middle frequencies, α is a time constant, meaning the time for diffusion, and S is an exponent related with the roughness of the diffusion media.

CPE is a constant phase element, which replaces the *C* element to have a better fit and represents the system behavior due to effects such as surface disorder, electrode porosity, and adsorption processes [60]. The impedance corresponding to *CPE* (Z_{CPE}) can be written as **Equation 6** [61]:

$$Z_{CPE} = \frac{1}{(j\omega)^n Y_0} \quad (6)$$

where Y_0 is the numerical value of the admittance, n is the *CPE* parameter, and ω ($\omega = 2\pi f$) is the angular frequency at the lowest frequency (f) measured in the impedance spectrum. Capacitance associated with *CPE* (C_{CPE}) can be evaluated using **Equation 7**:

$$C_{CPE} = \frac{Y_0}{\omega^{n-1}\sin(n\pi/2)} \quad (7)$$

Parameter values obtained from the EIS data fitting using ZVIEW software are presented in **Table 4**.

Table 4 Parameters values from the simulation of the EIS Data.

Parameters	**ESD Gr/AC/ cellulose-based separator**
***ESR* (Ω)**	1.69
R_{EI} **(Ω)**	3.16
CPE_{EI} **(Y_o [$\Omega^{-1}s^n$])**	4.22E-6
(*n*)	0.6
R_{ct} **(Ω)**	814.1
CPE_{dl} **(Y_o [$\Omega^{-1}s^n$])**	7.1E-3
(*n*)	0.6
***W* (R_w)**	284.9
(s)	5.84

(a)	0.5
CPE$_{ps}$ **(Y_o [$\Omega^{-1}s^n$])**	9.87E-3
(*n*)	0.6

The *ESR* and R_{ct} values for the ESD were 1.68 Ω and 3.18 Ω, respectively; the low *ESR* and R_{ct} values are responsible for the high ionic conductivity electrolyte [50] and higher ion diffusion [62], respectively. The value n=0.6 for the CPE_{dl}, suggests a capacitive behavior for the interfacial phenomena. The n value < 1 (ideal capacitor) can be associated with the heterogeneities of the electrode surface [63]. Furthermore, n=0.6 for the CPE_{ps}, showing that the kinetics of the electrode is limited by diffusion and migration of K^+ ions in the liquid electrolyte [64].

From the Z_{im} component, the capacitance (C) of the devices was calculated at 20 kHz using **Equation 8** [65]:

$$C = -1 / \omega Z_{im} \quad (8)$$

Where, ω is the angular frequency = $2\pi f$ (in Hz used for EIS measurements). The C value was 0.353 F and specific capacitance (C_s) = 15.37 F g^{-1}. This value is like C_{CV} (17.3 Fg^{-1}) at 10, mVs^{-1} indicating very similar device capabilities in the unstable (CV) and very stable (EIS) states of the electrode.

Figure 17 shows the charge and discharge curve for the ESD. The device reached the source voltage in a time determined by 5τ, where τ = RC. Likewise, the device was discharged until it had almost 0V at the same time determined by τ. This charge and discharge graph shows that the manufactured device stored energy, and its curve is characteristic of a capacitor [66, 67]. The calculated value of the capacitance was 10.7 μF. A video with the charge/discharge process is presented in supporting information.

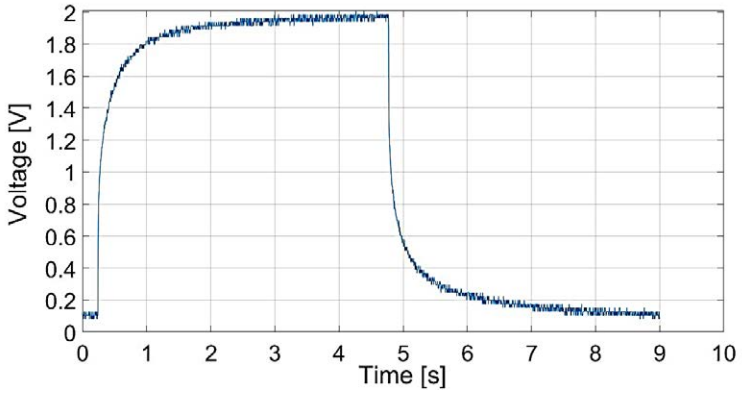

Figure 17 Voltage profile of a charge/discharge cycle of the ESD in 3M KOH electrolyte and current density = 0.2 A cm^{-2}.

4. Conclusions

Sodium alginate, cellulose and nanocellulose were extracted from sargassum collected from the beaches of the Mexican Caribbean; the IR spectra for the extracted materials were very similar to the IR spectra of commercial materials. The yields in the extraction processes were: 20% and 39%, for sodium alginate, and 13% and 37% for cellulose and nanocellulose, respectively. The yields obtained in the processes for the synthesis of the materials are very promising compared to some yields reported in the literature, indicating that the parameters used in the processes of the present study are suitable for the synthesis of sodium alginate, cellulose and nanocellulose from sargassum. Likewise, the physicochemical characterization of sargassum showed interesting results for the use of this macroalgae in the generation of bioenergy and removal of toxic contaminants from aquatic environments. The electrochemical and electrical characterization of the energy storage devices based on graphite and activated carbon, and manufactured with the cellulose-based separator, showed that it is feasible to manufacture a separator from sargassum for its application in energy storage devices due to specific capacitance values obtained and observed behaviors in the EIS, CV, and oscilloscope.

5. Declaration of competing interest

We declare that we have no significant competing interests including financial or non-financial, professional, or personal interests interfering with the full and objective presentation of the work described in this manuscript.

6. Acknowledgement

Adriana Cervantes-Mendiola, M.E. Nicho and U. León-Silva thank the CONACyT / México for the 2023-000002-01NACF-04483 doctoral scholarship for Adriana Cervantes-Mendiola.

7. Author contributions

A. Cervantes-Mendiola: methodology, investigation, formal analysis and writing original draft. U. León-Silva.: conceptualization, investigation, writing-original draft and project administration. M. E. Nicho.: Investigation and formal analysis. J. Escobedo-Alatorre: Investigation and formal analysis. A. Sandoval-Espino: methodology, investigation, formal analysis, writing original draft. A. Olarte-Paredes.: Investigation and formal analysis. All authors participated in writing the manuscript.

8. Data availability statement

The associated raw data is available at: León, Ulises (2024), “Sargassum”, Mendeley Data, V1, doi: 10.17632/n76vzdvpg8.1

References

[1] C. Hernández-Navarro, S. Pérez, E. Flórez, N. Acelas, and J. Muñoz-Saldaña, "Sargassum macroalgae from Quintana Roo as raw material for the preparation of high-performance phosphate adsorbent from aqueous solutions," *J. Environ. Manage.*, vol. 342, p. 118312, 2023, doi: https://doi.org/10.1016/j.jenvman.2023.118312.

[2] R. E. Rodríguez-Martínez, E. G. Torres-Conde, and E. Jordán-Dahlgren, "Pelagic Sargassum cleanup cost in Mexico," *Ocean Coast. Manag.*, vol. 237, no. 106542, 2023, doi: https://doi.org/10.1016/j.ocecoaman.2023.106542.

[3] V. Chávez *et al.*, "Massive influx of pelagic sargassum spp. On the coasts of the Mexican Caribbean 2014–2020: Challenges and opportunities," *Water (Switzerland)*, vol. 12, no. 10, pp. 1–24, 2020, doi: 10.3390/w12102908.

[4] M. Wang, C. Hu, B. B. Barnes, G. Mitchum, B. Lapointe, and J. P. Montoya, "The great Atlantic Sargassum belt," *Science (80-.).*, vol. 364, no. 6448, pp. 83–87, 2019, doi: 10.1126/science.aaw7912.

[5] K. Bilba, C. Onésippe Potiron, and M. A. Arsène, "Invasive biomass algae valorization: Assessment of the viability of Sargassum seaweed as pozzolanic material," *J. Environ. Manage.*, vol. 342, no. May, 2023, doi: 10.1016/j.jenvman.2023.118056.

[6] A. Ahmad *et al.*, "A critical review on the synthesis of natural sodium alginate based composite materials: An innovative biological polymer for biomedical delivery applications," *Processes*, vol. 9, no. 1, pp. 1–27, 2021, doi: 10.3390/pr9010137.

[7] A. Mohammed *et al.*, "Multistage extraction and purification of waste Sargassum natans to produce sodium alginate: An optimization approach," *Carbohydr. Polym.*, vol. 198, pp. 109–118, 2018, doi: 10.1016/j.carbpol.2018.06.067.

[8] A. R. Gordillo Sierra, L. F. Amador-Castro, A. E. Ramírez-Partida, T. García-Cayuela, D. Carrillo-Nieves, and H. S. Alper, "Valorization of Caribbean Sargassum biomass as a source of alginate and sugars for de novo biodiesel production," *J. Environ. Manage.*, vol. 324, p. 116364, 2022, doi: https://doi.org/10.1016/j.jenvman.2022.116364.

[9] P. Kumar Gupta *et al.*, *An Update on Overview of Cellulose, Its Structure and Applications*. IntechOpen, 2019.

[10] Y. Chao *et al.*, "Ordinary filter paper-derived hierarchical pore structure carbon materials for supercapacitor," *J. Energy Storage*, vol. 35, p. 102331, 2021, doi: https://doi.org/10.1016/j.est.2021.102331.

[11] L. Zhang *et al.*, "Flexible Asymmetrical Solid-State Supercapacitors Based on Laboratory Filter Paper," *ACS Nano*, vol. 10, no. 1, pp. 1273–1282, Jan. 2016, doi: 10.1021/acsnano.5b06648.

[12] S. Jiao *et al.*, "A Facile Method of Preparing the Asymmetric Supercapacitor with Two Electrodes Assembled on a Sheet of Filter Paper," *Nanomaterials*, vol. 9, no. 9, 2019, doi: 10.3390/nano9091338.

[13] H. Ma, Z. Cheng, X. Li, B. Li, Y. Fu, and J. Jiang, "Advances and challenges of cellulose functional materials in sensors," *J. Bioresour. Bioprod.*, vol. 8, no. 1, pp. 15–32, 2023, doi: https://doi.org/10.1016/j.jobab.2022.11.001.

[14] H. Doh, M. H. Lee, and W. S. Whiteside, "Physicochemical characteristics of cellulose

nanocrystals isolated from seaweed biomass," *Food Hydrocoll.*, vol. 102, 2020, doi: 10.1016/j.foodhyd.2019.105542.

[15] L. Dagousset, G. Pognon, G. T. M. Nguyen, F. Vidal, S. Jus, and P.-H. Aubert, "Self-standing gel polymer electrolyte for improving supercapacitor thermal and electrochemical stability," *J. Power Sources*, vol. 391, pp. 86–93, 2018, doi: https://doi.org/10.1016/j.jpowsour.2018.04.073.

[16] X. Aeby, A. Poulin, G. Siqueira, M. K. Hausmann, and G. Nyström, "Fully 3D Printed and Disposable Paper Supercapacitors," *Adv. Mater.*, vol. 33, no. 26, p. 2101328, 2021, doi: https://doi.org/10.1002/adma.202101328.

[17] A. Rafique *et al.*, "A facile blow spinning technique for green cellulose acetate/polystyrene composite separator for flexible energy storage devices," *Chem. Eng. J.*, vol. 464, p. 142515, 2023, doi: https://doi.org/10.1016/j.cej.2023.142515.

[18] D. Zhao *et al.*, "Highly Flexible and Conductive Cellulose-Mediated PEDOT:PSS/MWCNT Composite Films for Supercapacitor Electrodes," *ACS Appl. Mater. Interfaces*, vol. 9, no. 15, pp. 13213–13222, Apr. 2017, doi: 10.1021/acsami.7b01852.

[19] S. Yang and X. Qian, "Conductive PPy@cellulosic Paper Hybrid Electrodes with a Redox Active Dopant for High Capacitance and Cycling Stability," *Polymers (Basel).*, vol. 14, no. 13, 2022, doi: 10.3390/polym14132634.

[20] H. Qiang, W. He, F. Guo, J. Cao, R. Wang, and Z. Guo, "Layer-by-Layer Self-Assembled TEMPO-Oxidized Cellulose Nanofiber/Reduced Graphene Oxide/Polypyrrole Films for Self-Supporting Flexible Supercapacitor Electrodes," *ACS Appl. Nano Mater.*, vol. 5, no. 5, pp. 6305–6315, May 2022, doi: 10.1021/acsanm.2c00397.

[21] X. Lin, M. Wang, J. Zhao, X. Wu, J. Xie, and J. Yang, "Super-tough and self-healable all-cellulose-based electrolyte for fast degradable quasi-solid-state supercapacitor," *Carbohydr. Polym.*, vol. 304, p. 120502, 2023, doi: https://doi.org/10.1016/j.carbpol.2022.120502.

[22] O. S. R. Pasanda and A. Azis, "THE EXTRACTION OF BROWN ALGAE (Sargassum sp) THROUGH CALCIUM PATH TO PRODUCE SODIUM ALGINATE," *J. Bahan Alam Terbarukan*, vol. 7, no. 1, pp. 64–69, 2018, doi: 10.15294/jbat.v7i1.11412.

[23] C. Yamashita, I. C. Freitas Moraes, A. G. Ferreira, C. C. Zanini Branco, and I. G. Branco, "Multi-response optimization of alginate bleaching technology extracted from brown seaweeds by an eco-friendly agent," *Carbohydr. Polym.*, vol. 251, no. August 2020, p. 116992, 2021, doi: 10.1016/j.carbpol.2020.116992.

[24] R. S. Baghel, C. R. K. Reddy, and R. P. Singh, "Seaweed-based cellulose: Applications, and future perspectives," *Carbohydr. Polym.*, vol. 267, p. 118241, 2021, doi: https://doi.org/10.1016/j.carbpol.2021.118241.

[25] J. A. Hernández-Flores *et al.*, "Morphological and Electrical Properties of Nanocellulose Compounds and Its Application on Capacitor Assembly," *Int. J. Polym. Sci.*, vol. 2020, p. 1891064, 2020, doi: 10.1155/2020/1891064.

[26] M. M. Rahman, P. M. Joy, M. N. Uddin, M. Z. Bin Mukhlish, and M. M. R. Khan, "Improvement of capacitive performance of polyaniline based hybrid supercapacitor," *Heliyon*, vol. 7, no. 7, 2021, doi: 10.1016/j.heliyon.2021.e07407.

[27] I. A. Nava-JimÃ\copyrightnez, S. Tejeda-Vega, G. E.- Cortina-RamÃ\-rez, G. ZarazÃ\textordmasculinea-Ortega, C. Berriozabal-Islas, and H. SÃ!`nchez-HernÃ!`ndez, "Macro and microelement analysis of Sargassum fluitans and Sargassum natans arriving in the coastal zone of Cancun, Quintana Roo, Mexico," *Rev. Biol. Mar. y Oceanogr.*, vol. 57,

pp. 26–33, 2022, [Online]. Available: http://www.scielo.cl/scielo.php?script=sci_arttext&pid=S0718-19572022000100026&nrm=iso.

[28] J. Tomailla and J. Iannacone, "Lethal and sublethal toxicity of arsenic, cadmium, mercury and lead on fish Paracheirodon innesi neon tetra (Characidae)," *Rev. Toxicol.*, vol. 35, pp. 95–105, 2019.

[29] A. Carmona Cerda, R., Urzúa Moll, *Caracterización de biomasa leñosa con fines energéticos*. BIOCOMSA : Facultad de Ciencias Forestales y de la Conservación de la Naturaleza : InnovaChile, 2013.

[30] R. Castro, J. Suárez, and F. Maseda Eimil, "Evaluación del poder calorífico superior en biomasa," *Investig. Agrar. Sist. y Recur. For.*, vol. No. 8, no. 1, pp. 129–138, 1999.

[31] L. S. Gasca Ferreyra, "Análisis cinético de la descomposición térmica de Sargassum spp como fuente renovable de energía," Universidad Michoacana de San Nicolás de Hidalgo, 2022.

[32] A. Cruz Montelongo, Carlos De la y Herrera Gamboa, Jaime y Ortiz Sánchez, Ixchel Abby y Ríos Saucedo, Julio César y Rosales Serna, Rigoberto y Carrillo-Parra, "Caracterización energética del carbón vegetal producido en el Centro Norte de México," *Madera y bosques*, vol. 26, no. 2, 2020.

[33] M. García, "Carbón de encino: fuente de calor y energía. CONABIO.," *Biodiversitas*, vol. 77, pp. 7–9, 2008.

[34] B. I. van Tussenbroek *et al.*, "Severe impacts of brown tides caused by Sargassum spp. on near-shore Caribbean seagrass communities," *Mar. Pollut. Bull.*, vol. 122, no. 1, pp. 272–281, 2017, doi: https://doi.org/10.1016/j.marpolbul.2017.06.057.

[35] S. Saldarriaga-Hernandez, E. F. Nájera-Martínez, M. A. Martínez-Prado, and E. M. Melchor-Martínez, "Sargassum-based potential biosorbent to tackle pollution in aqueous ecosystems – An overview," *Case Stud. Chem. Environ. Eng.*, vol. 2, p. 100032, 2020, doi: https://doi.org/10.1016/j.cscee.2020.100032.

[36] D. M. S. A. Salem and M. M. Ismail, "Characterization of cellulose and cellulose nanofibers isolated from various seaweed species," *Egypt. J. Aquat. Res.*, vol. 48, no. 4, pp. 307–313, 2022, doi: https://doi.org/10.1016/j.ejar.2021.11.001.

[37] Y. Ore B., E. R. Pichilingue L, and A. C. Valderrama Negrón, "EXTRACCIÓN Y CARACTERIZACIÓN DEL ALGINATO DE SODIO DE LA MACROALGA Macrocystis pyrifera," *Rev. la Soc. Química del Perú*, vol. 86, no. 3, pp. 276–287, 2020, doi: 10.37761/rsqp.v86i3.300.

[38] J. M. Wasikiewicz, F. Yoshii, N. Nagasawa, R. A. Wach, and H. Mitomo, "Degradation of chitosan and sodium alginate by gamma radiation, sonochemical and ultraviolet methods," *Radiat. Phys. Chem.*, vol. 73, no. 5, pp. 287–295, 2005, doi: https://doi.org/10.1016/j.radphyschem.2004.09.021.

[39] H. Daemi and M. Barikani, "Synthesis and characterization of calcium alginate nanoparticles, sodium homopolymannuronate salt and its calcium nanoparticles," *Sci. Iran.*, vol. 19, no. 6, pp. 2023–2028, 2012, doi: https://doi.org/10.1016/j.scient.2012.10.005.

[40] M. F. Nazarudin *et al.*, "Metabolic variations in seaweed, Sargassum polycystum samples subjected to different drying methods via 1H NMR-based metabolomics and their bioactivity in diverse solvent extracts," *Arab. J. Chem.*, vol. 13, no. 11, pp. 7652–7664, 2020, doi: https://doi.org/10.1016/j.arabjc.2020.09.002.

[41] C.-L. Mei-Lin Kok, Jamie and Wong, "In vitro Properties of Methanol Extract and Sodium Alginate of Sargassum polycystum C. Agardh Brown Seaweed Collected from Malaysia.," *Trop. Life Sci. Res.*, vol. 33, no. 1, 2022.

[42] H. N. Afifah and S. H. Putri, "Dewaxing Effects on Cellulose Isolation from Waste of Red Algae and Brown Algae," vol. 2, no. 1, pp. 127–134, 2024.

[43] L. Chávez-Guerrero, A. Toxqui-Terán, and O. Pérez-Camacho, "One-pot isolation of nanocellulose using pelagic Sargassum spp. from the Caribbean coastline," *J. Appl. Phycol.*, vol. 34, no. 1, pp. 637–645, 2022, doi: 10.1007/s10811-021-02643-5.

[44] Wu, Mingxia & Yang, Chongyang & Xia, Hengheng & Xu, Jiaqiang. (2021). Comparative analysis of different separators for the electrochemical performances and long-term stability of high-power lithium-ion batteries. Ionics. 27. 10.1007/s11581-021-03943-z.

[45] Xu, Quan & Kong, Qingshan & Liu, Zhihong & Wang, Xuejiang & Liu, Rongzhan & Zhang, Jianjun & Yue, Liping & Duan, Yulong & Cui, Guanglei. (2013). Cellulose/Polysulfonamide Composite Membrane as a High Performance Lithium-Ion Battery Separator. ACS Sustainable Chemistry & Engineering. 2. 194–199. 10.1021/sc400370h.

[46] Daman Xu, Yingqi Heng, Xiang Qin, Dongying Hu, Membrane-based symmetric supercapacitors composed of cellulose solution-derived polydopamine-modified separators and polypyrrole/graphene-doped polydopamine-modified electrodes, Journal of Energy Storage, Volume 50, 2022, https://doi.org/10.1016/j.est.2022.104640.

[47] Rodríguez-Quesada, J., Rodriguez Mora, K., Bernal-Samaniego, C.A., Jirón-García, E., & Rojas-Alvarado, C. (2024). Development of Nanocellulose Hydrogels from Sargassum Seaweed as Controlled Nutrient Release Systems and their Application in Germination. Ecological Engineering & Environmental Technology. DOI:10.12912/27197050/192775

[48] K. K. Yadav, R. Wadhwa, N. Khan, and M. Jha, "Efficient metal-free supercapacitor based on graphene oxide derived from waste rice," *Curr. Res. Green Sustain. Chem.*, vol. 4, p. 100075, 2021, doi: https://doi.org/10.1016/j.crgsc.2021.100075.

[49] X. Guo, Fenghua and Gupta, Nivedita and Teng, *Enhancing pseudocapacitive process for energy storage devices: analyzing the charge transport using electro-kinetic study and numerical modeling*, vol. 87. Books on Demand, 2018.

[50] S. B. Aziz, E. M. A. Dannoun, A. R. Murad, K. H. Mahmoud, M.A. Brza, M. M. Nofal, K. A. Elsayed, S. N. Abdullah, J. M. Hadi, M. F. Z. Kadir, "Influence of scan rate on CV Pattern: Electrical and electrochemical properties of plasticized Methylcellulose: Dextran (MC:Dex) proton conducting polymer electrolytes", *Alex. Eng. J*, vol. 61, no. 8, pp. 5919-5937, 2022. https://doi.org/10.1016/j.aej.2021.11.020.

[51] C. Kim, Y. S., Balland, V., Limoges, B., & Costentin, *Cyclic voltammetry modeling of proton transport effects on redox charge storage in conductive materials: application to a TiO 2 mesoporous film*, vol. 19, no. 27. 2017.

[52] K. M. Ajay and M. N. Dinesh, "Influence of various Activated Carbon based Electrode Materials in the Performance of Super Capacitor," *IOP Conf. Ser. Mater. Sci. Eng.*, vol. 310, no. 1, p. 12083, Feb. 2018, doi: 10.1088/1757-899X/310/1/012083.

[53] V. V. N. Obreja, A. Dinescu, and A. C. Obreja, "Activated carbon based electrodes in commercial supercapacitors and their performance," *Int. Rev. Electr. Eng.*, vol. 5, no. 1, pp. 272–281, 2010.

[54] A. H. Ab. Rahim, N. Ramli, A. N. Nordin, and M. F. Abd. Wahab, "Supercapacitor performance with activated carbon and graphene nanoplatelets composite electrodes, and insights from the equivalent circuit model," *Carbon Trends*, vol. 5, p. 100101, 2021, doi: https://doi.org/10.1016/j.cartre.2021.100101.

[55] G. Jochen, K. Julia, M. Sander, S. D. Uwe, "High-spatial impedance-based modeling of electrical and thermal behavior of lithium-ion batteries - A powerful design and analysis tool for battery packs in hybrid electric vehicles", Electric Drive Transportation Association - 23rd Int. Electric Vehicle Symposium and Exposition 2007, EVS 2007 (Battery, Hybrid, Fuel Cell) Conf. Proc. - Sustainability: The Future of Transportation. 3. 1331-1345.

[56] N. O. Laschuk, E. B. Easton, and O. V. Zenkina, "Reducing the resistance for the use of electrochemical impedance spectroscopy analysis in materials chemistry," *RSC Adv.*, vol. 11, no. 45, pp. 27925–27936, 2021, doi: 10.1039/d1ra03785d.

[57] B. Balu and A. S. Khair, "The electrochemical impedance spectrum of asymmetric electrolytes across low to moderate frequencies," *J. Electroanal. Chem.*, vol. 911, p. 116222, 2022, doi: https://doi.org/10.1016/j.jelechem.2022.116222.

[58] X. Fan, P. Ohlckers, and X. Chen, "Tunable Synthesis of Hollow Co3O4 Nanoboxes and Their Application in Supercapacitors," *Appl. Sci.*, vol. 10, no. 4, 2020, doi: 10.3390/app10041208.

[59] A. Habekost, "Fundamentals and Applications of Electrochemical Impedance Spectroscopy - A Didactic Perspective," *World J. Chem. Educ.*, vol. 9, no. 1, pp. 14–21, 2021, doi: 10.12691/wjce-9-1-3.

[60] J.-B. Jorcin, M. E. Orazem, N. Pébère, and B. Tribollet, "CPE analysis by local electrochemical impedance spectroscopy," *Electrochim. Acta*, vol. 51, no. 8, pp. 1473–1479, 2006, doi: https://doi.org/10.1016/j.electacta.2005.02.128.

[61] J. D. Huffstutler *et al.*, "High Performance Graphene-Based Electrochemical Double Layer Capacitors Using 1-Butyl-1-methylpyrrolidinium tris (pentafluoroethyl) trifluorophosphate Ionic Liquid as an Electrolyte," *Electronics*, vol. 7, no. 10, 2018, doi: 10.3390/electronics7100229.

[62] D. Gandla, H. Chen, and D. Q. Tan, "Mesoporous structure favorable for high voltage and high energy supercapacitor based on green tea waste-derived activated carbon," *Mater. Res. Express*, vol. 7, no. 8, 2020, doi: 10.1088/2053-1591/abaf40.

[63] P. M. H. Madhushanka, K. S. P. Karunadasa, R. M. Gamini Rajapakse, C. H. Manoratne, and H. M. N. Bandara, "Low-cost composite electrode consisting of graphite, colloidal graphite and montmorillonite with enhanced electrochemical performance for general electroanalytical techniques and device fabrication," *Chem. Pap.*, vol. 78, no. 1, pp. 633–643, 2024, doi: 10.1007/s11696-023-03086-7.

[64] A. Jagadale, X. Zhou, R. Xiong, D. P. Dubal, J. Xu, and S. Yang, "Lithium ion capacitors (LICs): Development of the materials," *Energy Storage Mater.*, vol. 19, pp. 314–329, 2019, doi: https://doi.org/10.1016/j.ensm.2019.02.031.

[65] A. Gomaa, Y. Mashitah, S. Essam, C. K. Feng, "High Performance MnO2 Nanoflower Supercapacitor Electrode by Electrochemical Recycling of Spent Batteries", *Ceram. Int.* vol. 43, pp. 8440-8448, 2017, https://doi.org/10.1016/j.ceramint.2017.03.195.

[66] S. Chandra Sekhar, B. Ramulu, and J. S. Yu, "Transition Metal Oxides for Supercapacitors BT - Nanostructured Materials for Supercapacitors," S. Thomas, A. B. Gueye, and R. K. Gupta, Eds. Cham: Springer International Publishing, 2022, pp. 267–292.
[67] J. H. Park, O. O. Park, K. H. Shin, C. S. Jin, and J. H. Kim, "An Electrochemical Capacitor Based on a Ni (OH) 2/Activated Carbon Composite Electrode," *Electrochem. Solid-State Lett.*, vol. 5, no. 2, p. H7, 2001, doi: 10.1149/1.1432245.